Research Article

Journal of Environmental Nanotechnology

Biosynthesis of Zinc Oxide Nanoparticles using *Cleome gynandra* Extract and Evaluation of its Cytotoxic Activities on A549 Cell Line

V. Velmani, M. Balaji, P. Rajesh*, G. T. Parethe and S. Kavica
PG & Research Department of Chemistry, Government Arts College (Autonomous), Coimbatore, TN, India
Received: 20.02.2024 Accepted: 27.03.2024 Published: 30.03.2024
*gacchemistryrajesh@gmail.com

ABSTRACT

Zinc oxide nanoparticles (ZnONPs) were green synthesised by a simple, rapid, eco-friendly and a cheaper method using *Cleome gynandra* plant extract. The ZnONPs were characterized using UV- Visible Spectroscopy, FT-IR, XRD, FE-SEM and EDX analysis. The formation of ZnONPs (355 nm) was confirmed by UV visible spectroscopy. The crystalline nature of the nanoparticles was studied by XRD. The presence of different functional groups in the biomolecules was evident from FT-IR spectrum. The morphology of ZnONPs was analysed using SEM and the presence of zinc oxide was confirmed through elemental analysis. They were also analyzed for their biological and antioxidant activities. The green synthesized ZnONPs exhibited a good antibacterial activity against both Gram-negative and Gram-positive bacteria. Furthermore, they exhibited appreciable anticancer activity on the lung (A549) cancer cell lines.

Keywords: *Cleome gynandra* plant extract; Zinc oxide nanoparticles; Antimicrobial activity; Antioxidant activity; Cytotoxic activity A549 cell line.

1. INTRODUCTION

The discovery of novel biocidal agents has resulted from recent developments in the field of nanotechnology, specifically the capacity to manufacture highly organized nanoparticulates of any size and shape. According to some reports, antibiotics can eradicate up to six distinct disease-causing organisms, but nanomaterials have the ability to eradicate up to 650 organisms (Gunalan *et al.* 2012). Green synthesis is a sustainable technology that has the potential to enable researchers worldwide to investigate the potential of numerous herbs for the synthesis of nanoparticles (Mubayi *et al.* 2012). Due to their huge surface area, shape, size and roughness, metal oxides are excellent candidates for bacterial interaction and can be highly effective as antimicrobials when incorporated into nanoparticles (Osonga *et al.* 2020). Zinc oxide nanoparticles (ZnONPs) have caused a lot of concern in recent studies since they have demonstrated significant potential in the treatment of cancer. Their capacity to create apoptosis and reactive oxygen particulate matter accounts for their potential (Mishra *et al.* 2017). The ZnONPs are also safe, nontoxic, and biocompatible, resulting in excellent choices for biological applications (Jamdagni *et al.* 2018). Physical as well as chemical methods have been used to manufacture the ZnO nanoparticles (Zhai *et al.* 2008). Plant extracts, microbes, and enzymes have all been proposed as potential environmentally benign substitutes for chemical and physical processes in the biological synthesis of ZnO nanoparticles (Awwad *et al.* 2014). The erect, glandular, pubescent annual herb *Cleome gynandra* is a member of the *Cleomaceae (Capparaceae)* family and is found in many tropical and subtropical regions of the world. It is widely employed in the *Siddha*, *Ayurvedic*, and folk medicines. It is known to in Tamil as *velai keerai*, *neivayalla keerai* or *kattu kadugu*, and in English as cat's whiskers or spider flower. The agricultural and nutritional systems of tropical and pantropical countries rely heavily on this wild, green crop (Chatterjee and Pakrashi,1991; Chweya and Mnzava, 1997; Van *et al.* 2007). This study aims to provide a low-cost, environmentally friendly method of synthesizing ZnONPs using extract from the *Cleome gynandra* plant that may display antimicrobial activity, antioxidant and cytotoxic activity.

2. EXPERIMENTAL

All the reagents and solvents were of analytical grade and used without any further purification. Commercially available zinc sulphate heptahydrate ($ZnSO_4.7H_2O$), sodium hydroxide (NaOH) and ethanol

were used. The fresh plant of *Cleome gynandra* was collected from Rasipuram, Namakkal District Tamil Nadu, India.

2.1 Preparation of Plant Extract

The fresh and healthy *Cleome gynandra* plants were collected, carefully cleaned with tap water, followed by distilled water and then dried for 15 days in a shed. After drying, the plant materials were ground into a powder. About 10 g of the powder was added to a flask containing 100 mL of double-distilled water, which was then heated for 1 hour at 60-80 ℃. The plant extract was cooled to room temperature and then filtered using Whatman filter paper No. 1. The final extract was stored at 4 ℃ for further use.

2.2 Synthesis of CG-ZnO Nanoparticles

For the green synthesis of the ZnONPs, 100 mL of an aqueous solution of 0.1 M ($ZnSO_4.7H_2O$) and the aqueous plant extract were stirred for 1 hour. NaOH solution (1 N) was added dropwise into the mixture to maintain the pH value at 12. The resultant white precipitate was washed with distilled water, followed by ethanol to remove the remaining impurities and dried in an oven 80 ℃ for 6 hours. The dried sample was then stored for characterization.

2.3 Characterization

An UV-Visible spectrometer (Perkin-Elmer lambda 19) was used to record the absorption measurements of nanoparticles. X-ray diffraction analysis was performed to investigate the crystalline properties and to calculate the average particle size. Fourier transform infrared (FT-IR) spectroscopic analysis was performed using a Perkin-Elmer spectrum RX-1 IR spectrophotometer within the range 4000 to 400 cm^{-1}. Surface morphology like shape, size, dispersed nature of nanoparticles and elemental composition of the sample was studied by scanning electron microscopy (SEM) embedded with EDX (energy dispersive x ray).

2.4 Antimicrobial Activity

The antimicrobial study was carried out by disc diffusion method using Muller-Hinton agar media (Bhumi and Savithramma, 2014). Amoxicillin and fluconazole were used as antimicrobial standard antibacterial and antifungal drugs, respectively. The test human bacterial pathogens (*Staphylococcus aureus*, *Staphylococcus epidermis*, *Pseudomonas aeruginosa* and *Klebsiella pneumonia*) and fungal pathogens (*Candida albicans*, *Candida vulgaris*, *Aspergillus niger* and *Aspergillus flavus*) were swabbed on to the surface of plated agar. Sterile filter paper disc loaded with various concentrations of sample of 60, 80 and 100 µg/ml were placed on the top of Mueller-Hilton agar plates. The plates were incubated at 37 ℃ for 24 hours and the zone of inhibition was recorded in millimetre and the experiments were run twice.

2.5 Antioxidant Activity

2.5.1 DPPH assay method

The antioxidant activity of CG-ZnONPs was examined by stable DPPH free radical activity (Acharya *et al.* 2004; Eva *et al*. 2003). Ethanolic solution of DPPH (0.05 mM) (500 µL) was added to 1000 µL of synthesized nanoparticle with different concentrations (20-100 µL). The freshly prepared DPPH solution was kept in the dark at 4 ℃. Then 96% (2.7 mL) of ethanol was added to the mixture and shaken vigorously. The mixture was allowed to stand for 5 minutes. The absorbance was measured spectrophotometrically at 540 nm. Absorbance was set to zero by using ethanol. A blank sample contains the same amount of ethanol and DPPH was prepared. The experiment was performed in triplicate. The radical activity of the tested samples, expressed as % of inhibition was calculated as follows.

$$\text{Percent (\%) inhibition of DPPH activity} = [(A-B)/A] \times 100$$

Here, A and B are absorbance values for blank and sample, respectively. A curve of concentration versus percentage inhibition was plotted and concentration required for 50% inhibition was determined.

2.6 Anticancer Activity

2.6.1 MTT assay

In cell viability assay, A549 viable cells were harvested and counted using haemocytometer. The cells were diluted in Dulbecco's Modified Eagle Medium (DMEM) to a density of 1×10^4 cells/ml, seeded in 96 well plates and incubated for 24 hours to allow attachment (Mosmann, 1983). After A549 cells were treated with control, different concentrations of CG-ZnONPs (1 to 10 µg/mL) were introduced to each well. The A549 cells were incubated at 37℃ in a humidified 95% air and 5% CO_2 incubator for 24 hours. After incubation, the drug-containing cells were washed with fresh culture medium and the MTT (5 mg/mL in PBS) dye was added to each well, followed by incubation for another 4 hours at 37℃. The purple precipitated formazan formed was dissolved in 100 µL of concentrated DMSO and the cell viability was assessed by measuring the absorbance at 540 nm using a multi-well plate reader. The results were expressed as percentage of stable cells with respect to the control. The half maximal inhibitory concentration (IC_{50}) values were calculated and the optimum doses were analysed at different time periods.

$$\text{Inhibition of cell proliferation (\%)} = \frac{\text{Mean absorbance of the control} - \text{Mean absorbance of the sample}}{\text{Mean absorbance of the control}} \times 100$$

The IC_{50} values were determined from the CG-ZnONPs dose responsive curve where inhibition of 50% cytotoxicity was compared to control cells. All experiments were performed at least three times in triplicate.

2.6.2 Measurement of apoptotic induction using acridine orange/ethidium bromide (AO/EB) dual staining method

Acridine orange (AO) is permeable and it stains all the A549 cells viable/nonviable cells. It emits green fluorescence if intercalated into double stranded nucleic acid (DNA) or red fluorescence if bound to single stranded nucleic acid (RNA) (Baskic *et al*. 2006). Ethidium bromide (EB) is taken up only by nonviable cells that have lost membrane integrity and emit red fluorescence by intercalation into DNA. Four types of cells were distinguished employing the fluorescence emission and the chromatin condensation of stained nuclei illustrated the morphological aspect. Viable cells have uniform bright green nuclei with an organized structure. Early apoptotic cells (which still have intact membranes but have started to undergo DNA cleavage) have green nuclei, but perinuclear chromatin condensation is visible as bright green patches or fragments. Late apoptotic cells have orange to red nuclei with condensed or fragmented chromatin. Necrotic cells have orange to red nuclei uniformly with no condensed chromatin.

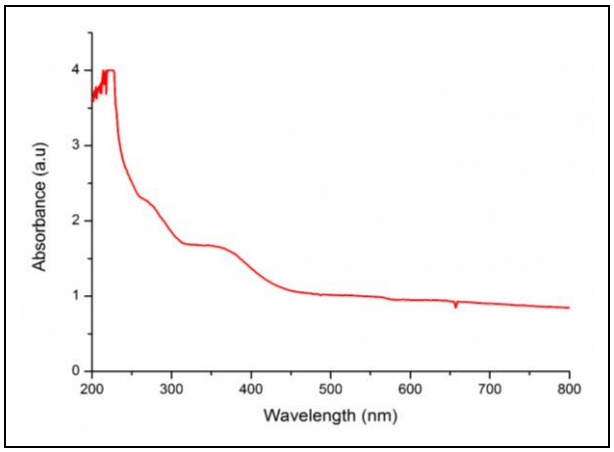

Fig. 1: UV-visible spectra of green synthesized CG-ZnO NPs

3. RESULTS AND DISCUSSION

3.1 UV-visible Spectroscopy Analysis

The synthesized CG-ZnONPs were examined using UV-visible spectroscopy. Strong electronic absorption was measured at 355 nm (Fig. 1), which is in accordance with the prominent quantum confinement effect of ZnO particles (Yong *et al.* 2010). At ambient temperature, ZnONPs showed a high excitation binding energy centred about 360 nm (Mohammadian *et al*. 2018).

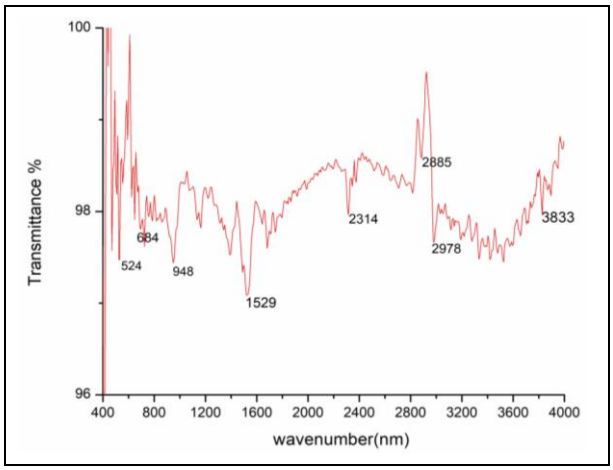

Fig. 2: FT-IR spectra of green synthesized CG-ZnO NPs

3.2 Fourier Transform Infrared Spectroscopy (FT-IR) Analysis

The FT-IR measurements showed the evidence of possible functional groups present in the synthesized CG-ZnONPs and helped in determining the role of aqueous extract in reducing the zinc sulphate into ZnONPs. The FT-IR spectrum is shown in Fig. 2. The two weak bands at 2978 cm^{-1} and 2885 cm^{-1} are attributed to the C-H stretching vibration of alkanes and O–H stretching vibration of the carboxylic group. Small peaks around 2314 cm^{-1} showed the presence of (-CN) nitrile group (Tas *et al*. 1998). The characteristic peak located at 648 cm^{-1} is due to the attachment of amide group and stretching mode of ZnO (Li *et al*. 2008). A sharp peak at 450 cm^{-1} confirmis Zn–O bending vibration (Nithya and Kalyanasundharam, 2019). The intensity of absorption in the 524 cm^{-1} clearly indicates a hexagonal phase of ZnO. The presence of phenolic groups and flavonoids in the extract of *Cleome gynandra* increases the production and stability of ZnO nanoparticles (Santhoshkumar *et al.* 2017). The band at 509 cm^{-1} corresponds to stretching frequency of Zn-O hexagonal phase (Reddy *et al.* 2011). The sharp peak at 524 and 470 cm^{-1} showed the characteristic stretching vibrational signals of ZnONPs. These vibrational peaks indicate that the plant extract contains phenols, polyphenols and primary amines, which took part in the reduction, capping and finally stabilization of ZnONPs. Similar observations of phytochemical assisted synthesis of

nanoparticles have also been made elsewhere shown to act as stabilizing agents, whereas the flavonoids act as capping agents (Yuvakkumar *et al*. 2015).

3.3 X-Ray Diffraction Analysis

The X-ray diffraction analysis helps to determine the crystal lattice, phases and the planes of the nanoparticles. In the present study, the diffraction peaks observed at 2θ values of 31.33º, 34.37º, 47.11º, 56.68º and 62.73º correspond to the Bragg's lattice plane of (100), (002), (101),(102), (110) and (103), respectively, with respect to "hkl" values (Fig. 3). The planes in the diffraction pattern of CG-ZnONPs confirmed the +2 oxidation state of zinc. Also, the diffraction pattern matched well with the JCPDS card number 36-1451 (Fan *et al*. 2014). The average crystalline size of the CG-ZnONPs calculated using Debye Scherrer's formula was found to be 15.20 nm. The crystal structure of the CG-ZnONPs was observed to be wurtzite hexagonal, as reported elsewhere (Darroudi *et al*. 2014).

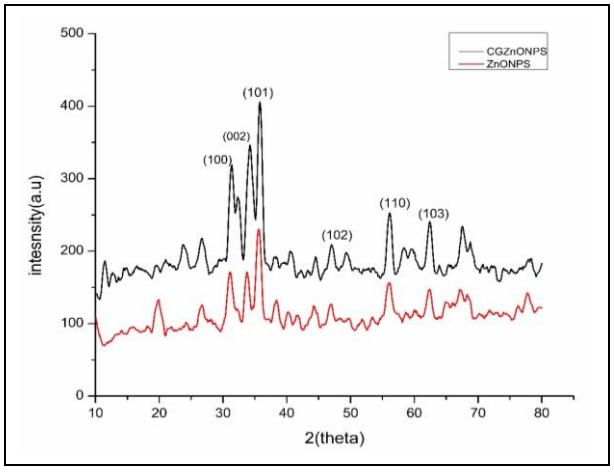

Fig. 3: XRD pattern of ZnO NPs and green synthesized CG-ZnO NPs

3.4 Energy Dispersive X-ray (EDX) and Scanning Electron Microscopy (SEM) Analysis

The EDX spectrum of CG-ZnO NPs (Fig. 4(a)) displays distinctive peaks of zinc at about 1 keV and oxygen at around 0.5 keV. The weight percentage distribution of the elements present in the nanomaterial is shown in the inset (b).

Figure 5 depicts the SEM image of ZnO NPs synthesized using plant extract of *C. gynandra* in two different magnifications. The particles were found to be substantially agglomerated, which may have resulted from the subsequent centrifugation and heating during the SEM preparations.

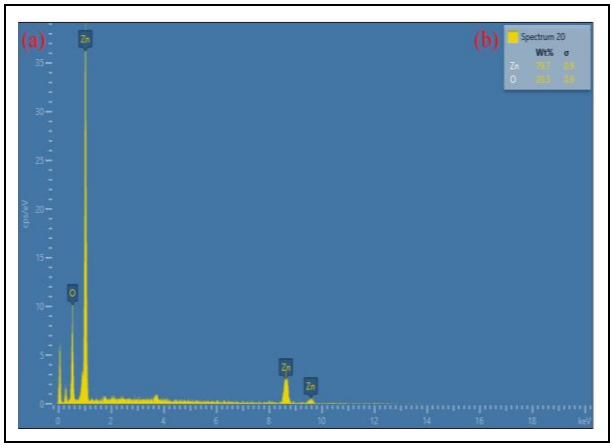

Fig. 4: (a) EDX pattern and (b- inset) Weight% distribution of elements in green synthesized CG-ZnO NPs

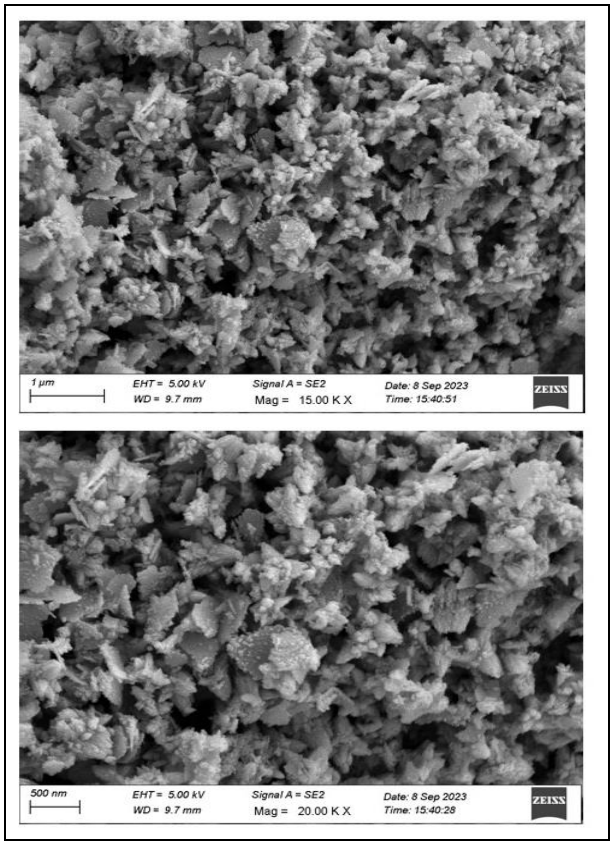

Fig. 5. SEM analysis of green synthesized CG-ZnONPs

3.5 Biological Activity of CG-ZnO Nanoparticles

The disc diffusion method was used to investigate the antibacterial activity of synthesized CG-ZnONPs against several kinds of pathogens, such as *Staphylococcus aureus*, *Staphylococcus epidermis*, *Pseudomonas aeruginosa* and *Klebsiella pneumonia*. For the comparative response, amoxicillin was used as the standard drug and the results are summarized in Table 1 and Fig. 6.

Table 1. Antibacterial activity (Zone of inhibition) by CG-ZnONPs

CG-**ZnONPs**	**Concentrations (µg/mL)**	**Organisms/Zone of inhibition (mm)**			
		S. aureus	***S. epidermis***	***P. aeruginosa***	***K. pneumonia***
	60	3	1	8	5
	80	6	2	9	6
	100	10	4	11	7
Standard (Std) (Amoxicillin)	10 µL/disc	12	10	13	14

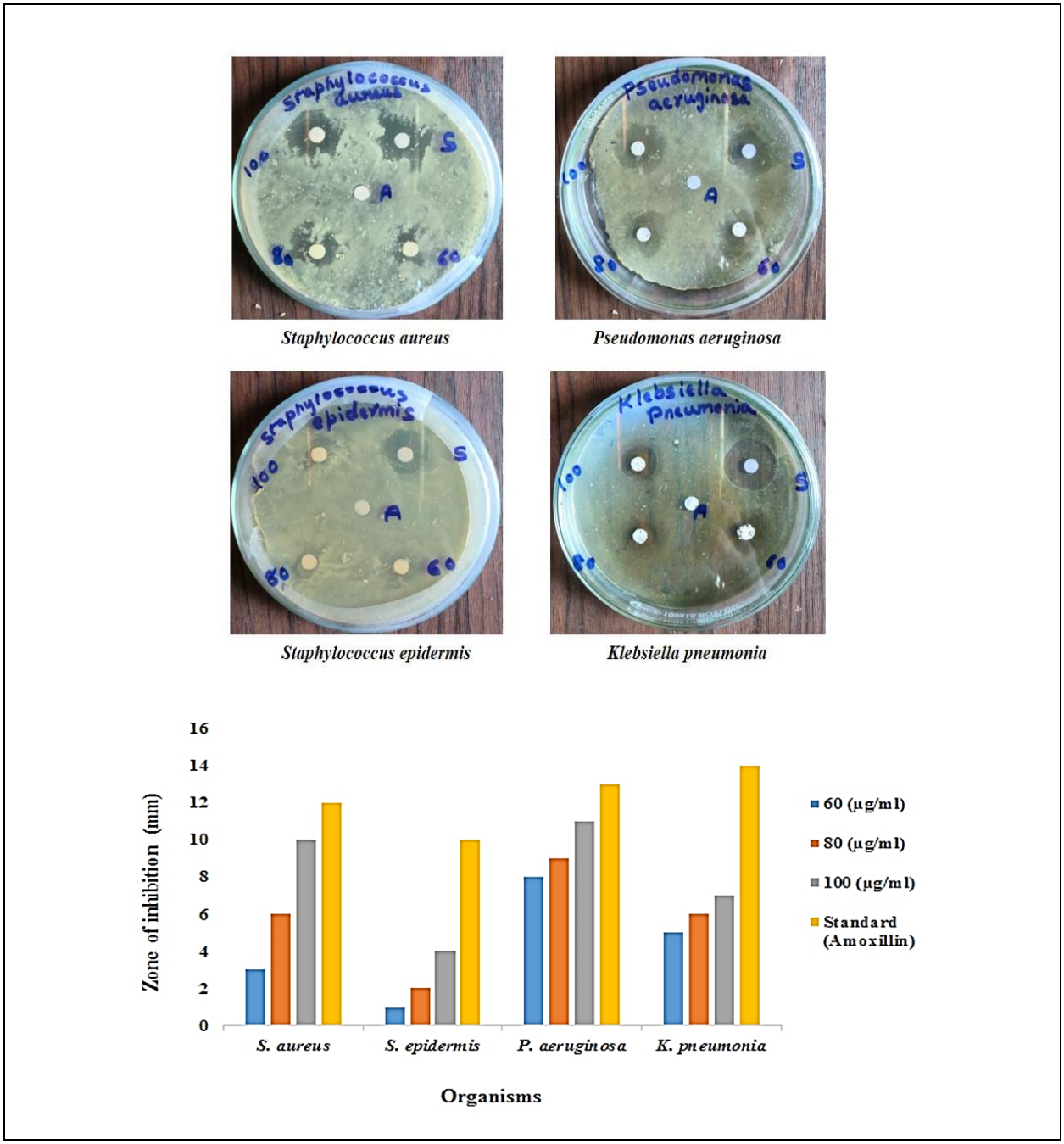

Fig. 6: Antibacterial activity of green synthesized CG-ZnONPs

Table 2. Antifungal activity (zone of inhibition) by CG-ZnONPs

CG-ZnONPs	Concentrations (µg/mL)	Organisms/Zone of inhibition (mm)			
		C. albicans	*C. vulgaris*	*A. niger*	*A. flavus*
	60	8	6	3	1
	80	9	7	4	4
	100	10	8	6	5
Standard (Std) (Fluconazole)	10 µL/disc	14	13	12	10

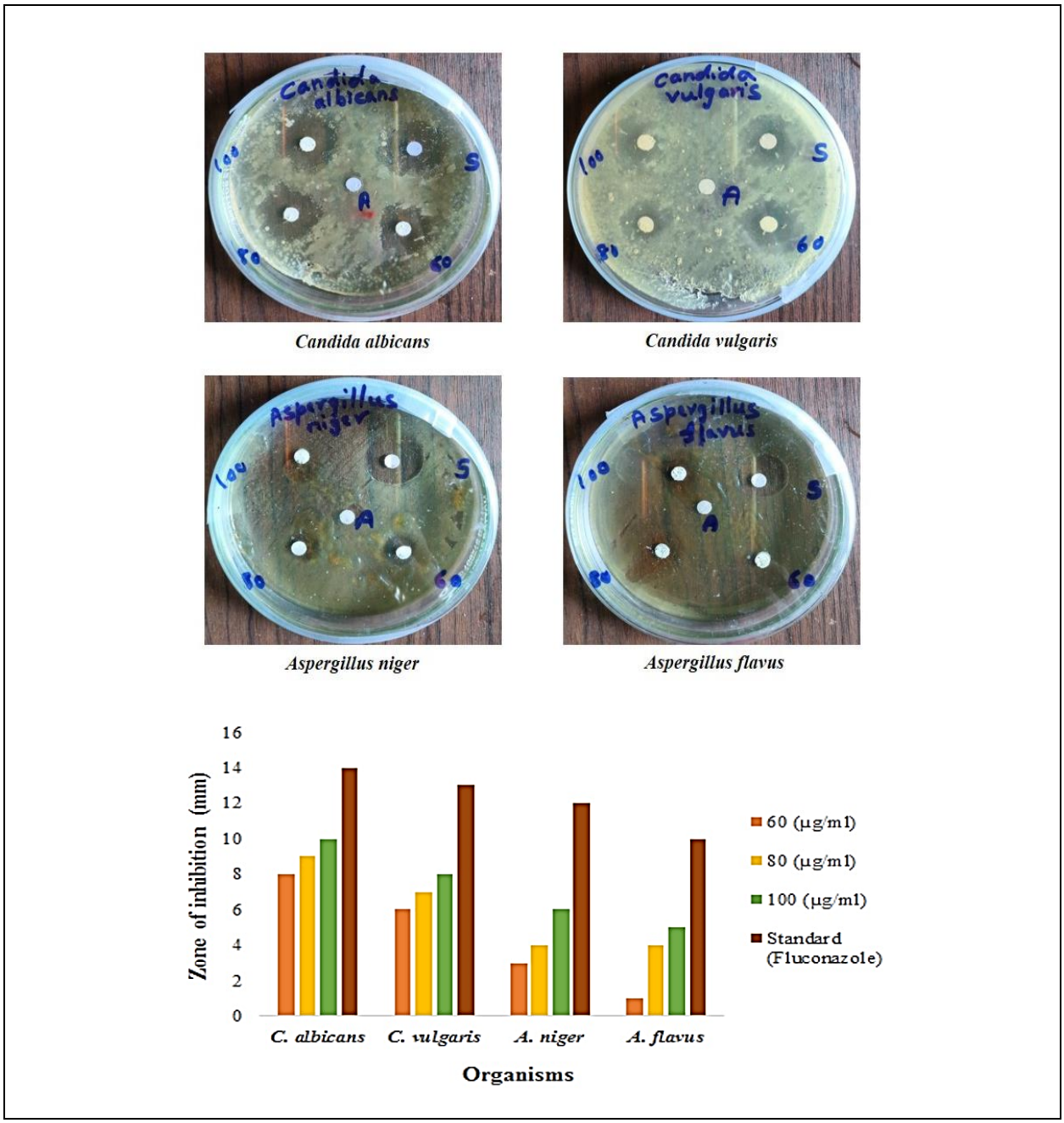

Fig. 7: Antifungal activity of CG-ZnONPs

ZnO nanoparticles were employed as positive and negative controls for the inhibitory study results, with concentrations of 60, 80 and 100 µg/mL serially diluted. At a maximum dose of 100 ppm, the highest inhibited area was found to be 11 mm against *Pseudomonas aeruginosa*, 10 mm against *Staphylococcus aureus*, 7 mm against *Klebsiella pneumonia* and 4 mm against *Staphylococcus epidermis*.

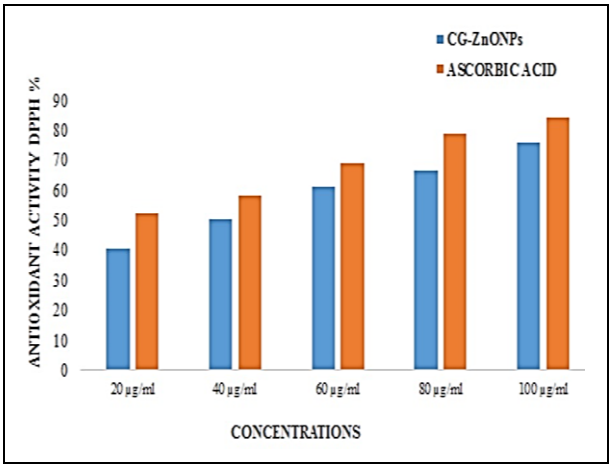

Fig. 8: Antioxidant activity of CG-ZnONPs by DPPH assay method

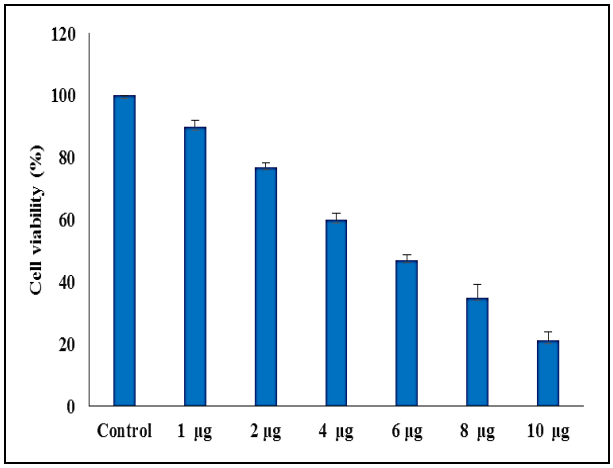

Fig. 10. Cytotoxic effect of CG-ZnONPs in lung cancer A549 cells

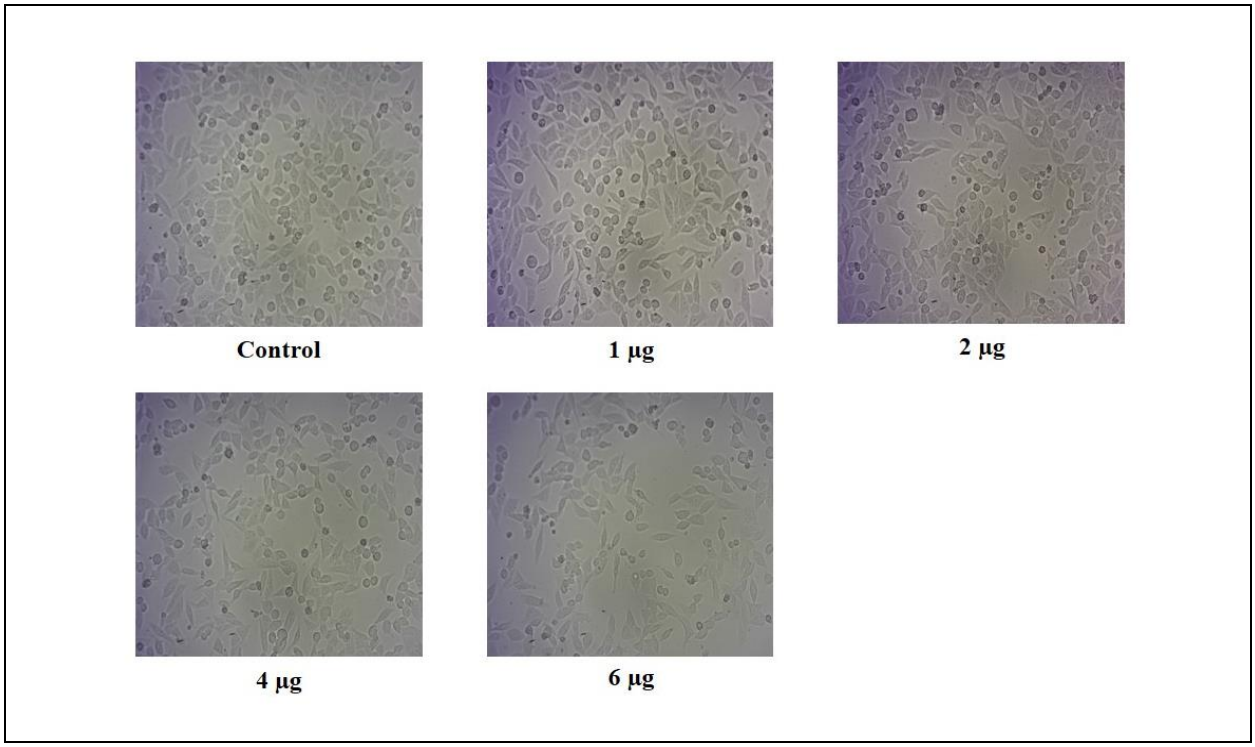

Fig. 9: Morphological changes in control and CG-ZnONPs treated lung cancer A549 cells observed for 24 hours

Similarly, the same method was used to test fungal strains including, *Candida albicans*, *Candida vulgaris*, *Aspergillus niger* and *Aspergillus flavus*. The results are displayed in Table 2. The zones of inhibition suggest good antifungal activity in comparison to standard fluconazole (Fig. 7). The antifungal activity of *Aspergillus flavus* is 5 mm, while the zone of inhibition for *Candida albicans*, *Candida vulgaris* and *Aspergillus niger* is 10 mm, 8 mm and 6 mm, respectively.

3.6 Antioxidant Activity

Antioxidants are assumed to possess an effect on DPPH owing to their hydrogen donating activity (Muthuvel *et al*. 2020). Due to its lipophilic nature, DPPH rapidly binds electrons from the antioxidant and turns yellow instead of violet. As a result, DPPH recognizes an electron or hydrogen intensity as a constant dynamic molecule together with a constant free radical. Figure 8 illustrates the findings on the impact of various CG-ZnONPs concentrations and ascorbic acid (standard) on the DPPH radical scavenging activity.

ZnONPs biosynthesized by the *C. gynandra* plant exhibited a scavenging rate ranging from 40.70% to 76.10% at concentrations of 20-100 µg/mL, while standard ascorbic acid showed a scavenging rate of

52.21% to 84.07%. Ascorbic acid demonstrated the highest radical scavenging ability with the lowest IC_{50} µg/mL (16.45) when compared to the green synthesized CG-ZnONPs. The green synthesized CG-ZnONPs had significant scavenging activity, with an IC_{50} µg/mL of 39.10. The higher potency of the nanoparticles for antioxidant activity is indicated by the lower IC_{50} µg/mL values. The DPPH free redical scavenging activity (IC_{50} µg/mL) for standard and green synthesized CG-ZnONPs at varying concentrations are displayed in Table 3.

Table 3. Antioxidant activity (Zone of inhibition) by CG-ZnO NPs

S. No.	Concentration (µg/ mL)	Antioxidant Activity DPPH %	
		CG-ZnO NPs	Ascorbic Acid
1.	20 µg/mL	40.70	52.21
2.	40 µg/ mL	50.44	58.40
3.	60 µg/ mL	61.06	69.02
4.	80 µg/ mL	66.37	78.76
5.	100 µg/ mL	76.10	84.07
	IC_{50} Value	39.10	16.45

3.7 *In vitro* Cytotoxicity

A549 cell lines were used in an *in vitro* approach for evaluating the cytotoxicity of the biosynthesized CG-ZnONPs. Using the MTT assay, the lung cancer cell lines were subjected to various doses of green synthesized CG-ZnONPs (1, 2, 4, 6, 8 and 10 mg mL^{-1}) for 24 hours. The outcomes were then contrasted with DMEM as the control. The cellular oxidoreductase enzymes that are dependent on NAD(P)H are responsible for the reduction of MTT reagent and other tetrazolium dyes, which changes their yellow color based on metabolic activity within cells (Berridge *et al*. 2005). Following the introduction of green synthesized CG-ZnONPs, substantial reductions in cell viability were noted, and an IC_{50} of 4 mg mL^{-1} was discovered. Following the treatment of A549 cell lines with green synthesized CG-ZnONPs, dead cells were seen in high density along with morphological alterations that defined the cytotoxic effect (Fig. 9).

3.8 Study of Apoptosis using CG-ZnO NPs by AO/EB Dual Staining

Further investigation into the morphological and biochemical alterations observed when CG-ZnONPs interacted with cells during the dose-dependent process towards A549 cells was carried out (Fig. 10). Through the use of dual staining, AO can penetrate both apoptotic and living cells by emitting green fluorescence, while EB stain can only enter necrotic cells by releasing red fluorescence (Mittal and Pandey, 2014; Das *et al*. 2017; George *et al*. 2018). The apoptotic cells emitted red fluorescence, which consisted entirely of dead cells (Nourmohammadi *et al*. 2019; Kanipandian *et al*. 2019; Sun *et al*. 2018). The observed morphological changes were caused in the A549 cells following treatment with the CG-ZnONPs. Fig. 11a shows the control. When the concentration of CG-ZnONPs increased, the number of living cells decreased and they interacted with dual stains to emit fluorescence (Fig. 11b, c). As illustrated in Fig. 11b, when AO/EB dye is applied to cell culture medium containing a 4 µg/mL test concentration of CG-ZnONPs, live cells absorbed the dye and produced green fluorescence, while dead cells showed red fluorescence. The dual staining test at 6 µg/mL test concentration of CG-ZnONPs in cell culture media is depicted in Fig. 11c. A red fluorescence is released by the dead cells (red dots), which shows a significant reduction in the number of live cells (green dots). The morphological alterations in the cell borders were not visible in Fig. 11a–c, but necrosis was present. The CG-ZnONPs have been shown to display anticancer properties against A549 cells, evidenced by the substantial number of dead cells produced by it.

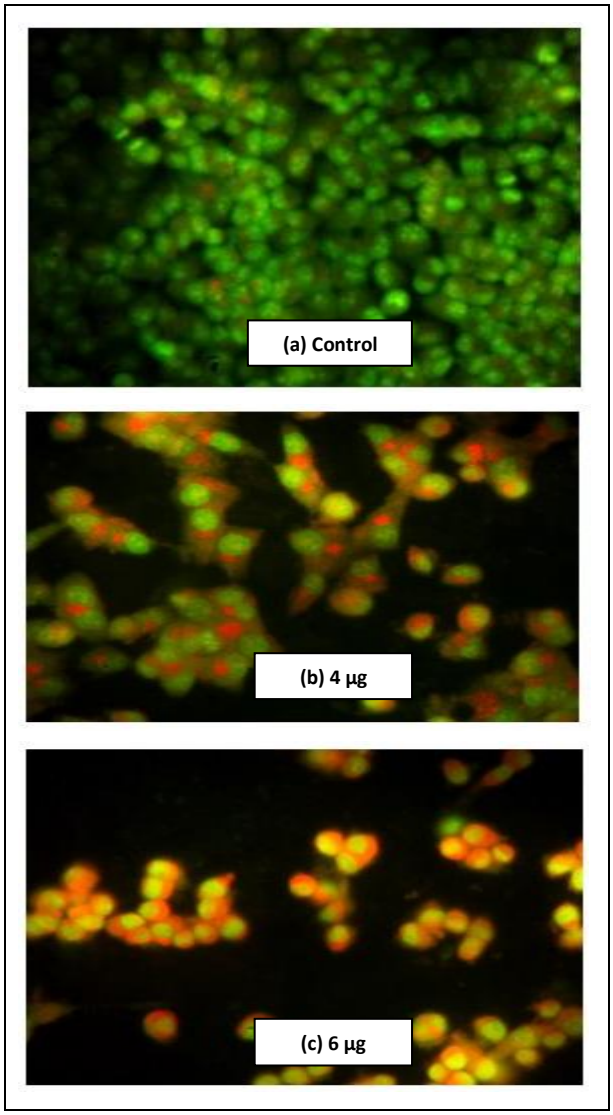

Fig. 11: Effect of CG-ZnONPs on the apoptotic cell death in the lung cancer A549 cells

4. CONCLUSION

ZnO nanoparticles were green synthesised using *C. gynandra* plant extract as a caping agent. The CG-ZnONPs nanoparticles were characterised by XRD, UV, FT-IR, SEM and EDX. The XRD measurements revealed an average crystallite size of 15.20 nm. The functional groups present in the ZnONPs were confirmed by FT-IR spectrum. The morphological characteristics were studied by FE-SEM. The EDX confirms the presence of ZnO compounds. The ZnONPs showed promising antimicrobial activities. The cytotoxic studies revealed dose-dependent suppression of lung cancer cell lines (A549) by CG-ZnONPs. Overall, the investigation suggests the possible biomedical applications of CG-ZnONPs.

FUNDING

This research received no specific grant from any funding agency in the public, commercial, or not-for-profit sectors.

CONFLICTS OF INTEREST

The authors declare that there is no conflict of interest.

REFERENCES

Acharya, K., Samui, K, Rai, M., Antioxidant and nitric oxide synthetase activation properties of *Auricularia auricular*, *Ind. J. Exp. Biol*., 42, 538-540 (2004).

Awwad, A. M., Albiss, B. and Ahmad, A. L., Green Synthesis, Characterization And Optical Properties Of Zinc Oxide Nanosheets Using Olea Europea Leaf Extract, *Adv. Mater. Lett.*, 5(9), 520-524 (2014). https://doi.org/10.5185/amlett.2014.5575

Baskic, D., Popovic, S., Ristic, P., Arsenijevic, N. N., Analysis of cyclohexamide-inducedapoptosis in human leukocytes: Fluorescence microscopy using annexin V/propidiumiodideversusacridin orange/ethidium bromide, *Cell Biol. Int.*, 30, 924-932 (2006). https://doi.org/10.1016/j.cellbi.2006.06.016

Berridge, M. V., Herst, P. M. and Tan, A.S., Tetrazolium dyes as tools in cell biology: new insights into their cellular reduction, *Biotechnol. Annu. Rev*., 11, 127–152 (2005). https://doi.org/10.1016/s1387-2656(05)11004-7

Bhumi, G. and Savithramma, N., Biological Synthesis of Zinc oxide Nanoparticles from Catharanthus roseus (l.) G. Don. Leaf extract and validation for antibacterial activity, *Int. J. Drug Dev. Res.*, 6(1), 208-214 (2014).

Chatterjee, A., Pakrashi, S. C., The Treatise on Indian Medicinal Plants, *Publications & Information Directorate*, New Delhi, 157-158 (1991).

Chweya, J. A., Mnzava, N. A., Cats whiskers, Cleome gynandra L: Promoting the conservation and use of underutilized and neglected crops, *Inst. Plant Genetics Crop Plant Res. Gaterleben/IPGRI*, Rome, Italy (1997).

Darroudi, M., Sabouri, Z., Oskuee, R.K., Zak, A. K., Kargar, H. and Abd, H. M. H. N., Green chemistry approach for the synthesis of ZnO nanopowders and their cytotoxic effects, *Ceram. Int.*, 40(3), 4827-4831 (2014). https://doi.org/10.1016/j.ceramint.2013.09.032

Das, J., Choi, Y. J., Han, J., Abu, M. M., Reza, T., Kim, J. H., Nanoceria-mediated delivery of doxorubicin enhances the anti-tumour efficiency in ovarian cancer cells via apoptosis, *Sci. Rep*., 7, 1-12 (2017). https://doi.org/10.1038/s41598-017-09876-w

Eva, S. B., Maria, H. T., Attila H., Csilla, R. and Ilona, S. V., Antioxidant effect of various rosemary (*Rosmarinus officinalis L.*) clones, *Acta Biologica Szegediensis*, 47(1), 111-113, (2003).

Fan, F., Feng, Y., Tang, P., Chen, A., Luo, R. and Li, D., Synthesis and Gas Sensing Performance of Dandelion-Like ZnO with Hierarchical Porous Structure, *Ind. Eng. Chem. Res.*, 53(32), 12737–12743 (2014). https://doi.org/10.1021/ie501825t

George, B., Kumar, N., Abrahamse, H. and Ray, S., Apoptotic efficacy of multifaceted biosynthesized silver nanoparticles on human adenocarcinoma cells, *Sci. Rep*., 8(1), 1-14 (2018). https://doi.org/10.1038/s41598-018-32480-5

Gunalan, S., Sivaraj, R. and Rajendran, V., Green synthesized ZnO nanoparticles against bacterial and fungal pathogens, *Progr. Nat. Sci.: Mater. Int.*, 22(6), 693-700 (2012). https://doi.org/10.1016/j.pnsc.2012.11.015

Jamdagni, P., Khatri, P. and Rana, J., Green synthesis of zinc oxide nanoparticles using flower extract of Nyctanthes arbor-tristis and their antifungal activity, *J. King Saud. Univ. Agric. Sci*., 30(2), 168-175 (2018). https://doi.org/10.1016/j.jksus.2016.10.002

Kanipandian, N., Li, D. and Kannan, S., Induction of intrinsic apoptotic signaling pathway in A549 lung cancer cells using silver nanoparticles from Gossypium hirsutum and evaluation of in vivo toxicity, *Biotechnol. Rep.*, 23, e00339–e00353 (2019). https://doi.org/10.1016/j.btre.2019.e00339

Li, G. Y., Jiang, Y. R., Huang, K., Ding, P. and Chen, J., Preparation and properties of magnetic Fe3O4–chitosan nanoparticles, *J. Alloys Compd.*, 466(1), 451-456 (2008). https://doi.org/10.1016/j.jallcom.2007.11.100

Mishra, P. K., Mishra, H., Ekielski, A., Talegaonkar, S. and Vaidya, B., Zinc oxide nanoparticles: a promising nanomaterial for biomedical applications, *Drug Discovery Today*, 22(12), 1825–1834 (2017). https://doi.org/10.1016/j.drudis.2017.08.006

Mittal, S. and Pandey, A., Cerium oxide nanoparticles induced toxicity in human lung cells: role of ROS mediated DNA damage and apoptosis, *Biomed. Res. Int.*, 2014, 1-15 (2014). https://doi. org/10.1155/2014/891934

Mohammadian, M., Eshaghi, Z. and Hooshmand, S., Green and chemical synthesis of zinc oxide nanoparticles and size evaluation by UV–vis spectroscopy, *J. Nanomed. Res.*, 7(1), 1-7 (2018).

Mosmann, T., Rapid colorimetric assay for cellular growth and survival: application to Proliferation and cytotoxicity assays, *J. Immunol. Methods*, 65(1), 55-63 (1983). https://doi.org/10.1016/0022-1759(83)90303-4

Mubayi, A., Chatterji, S., Rai, P. K. and Watal, G., Evidence Based Green Synthesis of Nanoparticles, *Adv. Mater. Lett.*, 3(6), 519-525 (2012). https://doi.org/10.5185/amlett.2012.icnano.353

Muthuvel, A., Jothibas, M. and Manoharan, C., Effect of chemically synthesis compared to biosynthesized ZnO-NPs using Solanum nigrum leaf extract and their photocatalytic, antibacterial and in-vitro antioxidant activity, *J. Environ. Chem. Eng.*, 8(2), 103705 (2020). https://doi.org/10.1016/j.jece.2020.103705

Nithya, K. and Kalyanasundharam, S., Effect of chemically synthesis compared to biosynthesized ZnO nanoparticles using aqueous extract of C. halicacabum and their antibacterial activity, Open Nano, 4, 100024 (2019). https://doi.org/10.1016/j.onano.2018.10.001

Nourmohammadi, E., Khoshdel, S. H., Nedaeinia, R., Sadeghnia, H. R., Hasanzadeh, L., Darroudi, M. and Kazemi, O. R., Evaluation of anticancer effects of cerium oxide nanoparticles on mouse fbrosarcoma cell line, *J. Cell. Physiol*., 234(4), 4987–4996 (2019). https://doi.org/10.1002/jcp.27303

Osonga, F. J., Akgul, A., Yazgan, I., Akgul, A., Eshun, G. B., Sakhaeeand, L., Sadik, O. A., *Molecules*, 25(11), 1-19 (2020). https://doi.org/10.3390/molecules25112682

Reddy, A. J., Kokila, M. K., Nagabhushana, H., Rao, J. L., Shivakumara, C., Nagabhushana, B. M. and Chakradhar, R. P. S., Combustion synthesis, characterization and Raman studies of ZnO nanopowders, *Spectrochim. Acta A Mol. Spectrosc*., 81(1), 53-58 (2011). https://doi.org/10.1016/j.saa.2011.05.043

Santhoshkumar, J., Kumar S. V. and Rajeshkumar, S., Synthesis of zinc oxide nanoparticles using plant leaf extract against urinary tract infection pathogen, *Resour.-Effic. Technol.*, 34(), 459-465 (2017). https://doi.org/10.1016/j.reffit.2017.05.001

Sun, H., Jia, J., Jiang, C. and Zhai, S., Gold nanoparticle-induced cell death and potential applications in nanomedicine, *Int. J. Mol. Sci*., 19, 754–774 (2018). https://doi.org/10.3390/ijms19030754

Tas, A. C., Chemical Preparation of the Binary Compounds in the Calcia-Alumina System by Self-Propagating Combustion Synthesis, *J. Am. Ceram. Soc.*, 81, 2853-2863 (1998). https://doi.org/10.1111/j.1151-2916.1998.tb02706.x

Van, D., Heever E, Venter, S. L., Nutritional and medicinal properties of *Cleome gynandra*, *Acta Hortic*., 752, 127–130 (2007). https://doi.org/10.17660/ActaHortic.2007.752.17

Yong, G., Gu, F., Han, D., Wang, Z. and Guo, G., Biomimetic Synthesis of Zinc Oxide 3D Architectures with Gelatin as Matrix, *J. Nanomater*., 2010, 1-7 (2010). https://doi.org/10.1155/2010/289173

Yuvakkumar, R., Suresh, J., Saravanakumar, B., Nathanael, A. J., Hong S. I. and V. Rajendran, Rambutan peels promoted biomimetic synthesis of bioinspired zinc oxide nanochains for biomedical applications, *Spectrochim. Acta, Part A*, 137, 250-258 (2015). https://doi.org/10.1016/j.saa.2014.08.022

Zhai, H. J., Wu, W. H., Lu, F., Wang, H. S. and Wang, C., Effects of ammonia and cetyltrimethylammonium bromide (CTAB) on morphologies of ZnO nano- and micromaterials under solvothermal process, *Mater. Chem. Phys.*, 112(3), 1024–1028 (2008). https://doi.org/10.1016/j.matchemphys.2008.07.020